18TH WORLD CONFERENCE ON EARTHQUAKE ENGINEERING
WCEE2024
MILAN

MILAN, ITALY
30TH JUNE - 5TH JULY 2024

www.wcee2024.it

FRAGILITY MODELING OF NUCLEAR POWER PLANTS' COMPONENTS: INTENSITY MEASURES AND DYNAMIC ANALYSIS SET-UP

G.Triantafyllou [1], I. Zentner [2], M. Kohrangi [3], A. Khemakem [4], V. Alves-Fernandes [2] & P. Bazzurro [5]

University School for Advanced Studies IUSS Pavia, Pavia, Italy georgios.triantafyllou@iusspavia.it

[2] Électricité de France, Paris-Saclay, France

[3] RED Risk, Engineering and Development, Pavia, Italy

[4] Électricité de France, UK Centre, Manchester, UK

[5] University School for Advanced Studies IUSS Pavia, Pavia, Italy

***Abstract**: In the framework of probabilistic seismic risk analysis (PRA) of nuclear power plants, a single ground motion intensity measure (IM) is generally used as a predictor of the performance of structures, systems, and components (SSCs) subject to earthquakes. In most cases, Peak Ground Acceleration (PGA) is the IM of choice. Several studies have shown, however, that the reliability assessment of SSCs can be improved by considering more than one IM because the different response measures of SSCs are sensitive to different IMs. Herein, we select different sets of ground motions using the Conditional Spectrum approach based on different conditioning IMs consistent with the hazard. We test the effects of the different sets on the floor response and the fragility estimation of SSC. We notice slight differences in the response and fragility computations when using different conditioning IMs. Moreover, we use the ground motion selected according to multiple stripe analysis (MSA) to derive fragility curves based on regression analysis. Then, we compare the differences between the two methods in deriving fragility curves. We observe little differences between regression and MSA. Finally, we discuss the option of incorporating Vector IMs in the seismic risk analysis of nuclear power plants.*

1. INTRODUCTION

This paper discusses some aspects of the methodology for understanding and quantifying the seismic risk of NPPs.

The methodology for seismic probabilistic risk assessment (SPRA, sometimes also called seismic probabilistic safety assessment, SPSA) can be summarized in 4 steps: Probabilistic seismic hazard analysis (PSHA), ground motion record selection and site response, SSC's response and fragility, and finally system risk analysis. In common practice, the structural response is assessed analytically (Step 2) by selecting ground motion records in agreement with the Uniform Hazard Spectrum (UHS) at the site (from Step 1) and other major intensity measures such as duration and Arias intensity.

An arguably more advanced analysis, however, would enforce more faithfully the consistency with the seismic hazard at the site at more than one intensity level by selecting ground motions based on either the conditional spectrum approach (CS) proposed by Jayaram et al. (2011), (a single target IM) or on the GCIM approach proposed by Bradley (2010) (multiple target IMs, including indicators other than spectral acceleration, Sa). First attempts to introduce this approach for nuclear applications are promising

(e.g.Trevlopoulos et al 2020) but are still to be refined and further studied to be ready for industrial applications.

These more advanced approaches, CS and GCIM, allow more than one IM to be considered and to include the statistical correlation among them during record selection. Bradley (2010) showed that considering only Sa ordinates, as standard in many conventional ground motion selection procedures, may result in ground motion sets misrepresentative of, for example, the duration features of the appropriate ground motion target. This is in line with practice in nuclear engineering where duration is part of the ground motion simulation or selection procedure. To more practically address this issue, other researchers (Spillatura *et al.*, 2021) have proposed a modification of the CS-based approach to account for Magnitude and source-to-site distance (i.e., M and R) during the ground motion selection. This technique uses hazard-consistent M and R values as proxies for ensuring that the distribution of not only duration but also of other IMs not directly covered by the spectral ordinates are appropriate for the site under consideration.

In nuclear engineering practice, PGA is often used as the IM for seismic PRA, and this means that hazard and fragility curves are developed for this scalar ground motion IM. In civil engineering where more conventional buildings and infrastructure are of interest, the framework of PBEE for the evaluation of seismic risk considers lower frequency spectral accelerations (Sa's) as scalar IM for hazard and fragility curves development. This is due to the better power of such IMs to predict the response of conventional buildings dominated by the content of ground motions at lower frequencies.

In this study, we will explore the sensitivity of the fragility curve of one SSC of a nuclear power plant to the conditioning IM selected to predict the SSC response and to the dynamic analysis set-up adopted to compute it. At the end we will also propose a methodology for assessing the risk to nuclear power plants SSCs using more than one ground motion intensity measure as response predictor and therefore using vector-valued (VPSHA) hazard analysis to support it.

2. CASE STUDY MODEL

2.1 Structural model of reactor building

The reactor building consists of a containment and an outbuilding located on a common foundation. The sealed cylindrical shell with an inner diameter of 45.0 m is located centrally, symmetrically in the outbuilding, measuring 66.0 x 66.0 meters. A reinforced concrete foundation slab of 2.4 meters in thickness is located under the reactor compartment.

The 3D view of the structural model built in Salome-meca (Delmas and Assire, 2009) and Code-Aster (Code-Aster, 2015) is illustrated in Figure 1. The model was created in the framework of the METIS project and, herein, we use this model as a case study. It is comprised of a mesh of triangular finite elements (FE) that uses 2D linear interconnected shell elements (Figure *2*). The model consists of 2800 nodes, with a maximum distance of 7 meters from one another.

The results of the modal analysis are presented in Table 1. The first mode in the x direction has a frequency of 4.05Hz and an effective mass participation of 44%, while the first mode in the y direction has a frequency of 3.9Hz and an effective participation mass of 40%. The first vertical mode has a frequency of 8.6Hz and corresponds to the vertical vibration of the dome. Figure 3 displays the first two mode shapes in x and y directions.

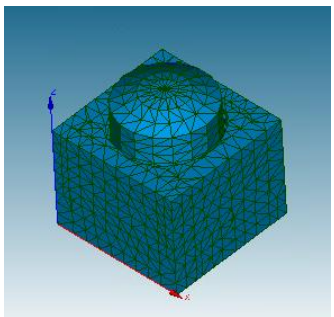

Figure 1: Finite element model mesh visualization

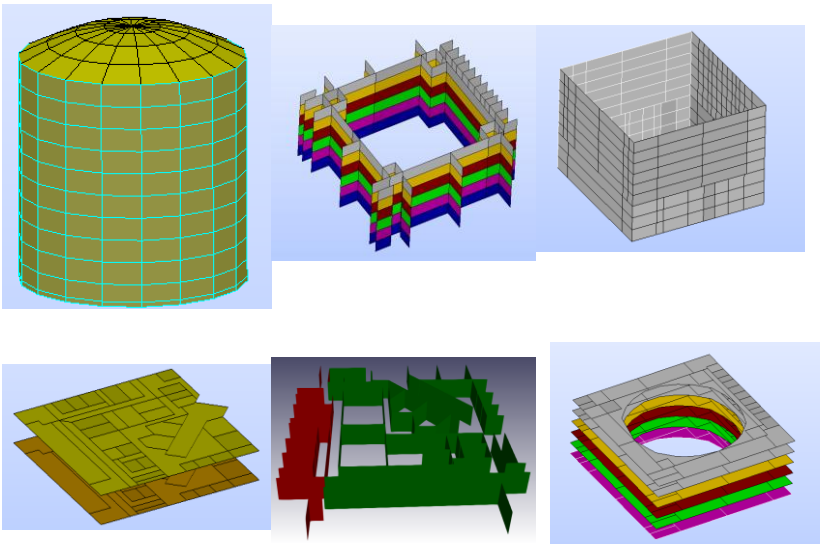

Figure 2: Geometry of different parts of the FE mode

Table 1: Modal analysis result

# of mode	frequency (Hz)	Effective mass participation (x)	Effective mass participation (y)	Effective mass participation (z)
1	3.89	8.17e-02	5.08e-01	2.24e-04
2	4.05	4.43e-01	8.38e-02	3.86e-08
…	…	…	…	…
7	8.61	2.50e-05	1.67e-03	1.24e-01

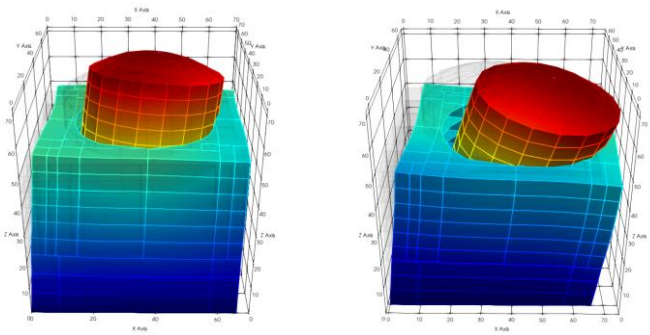

Figure 3: Mode shapes visualized in Salome-meca; 1st mode y-direction (left) and 1st mode in x-direction (right)

Note that a few modelling simplifications have been adopted: the tendons of the dome, the cylindrical part and the nuclear reactor's internal parts, including walls and floors, have not yet been included in the model. These shortcomings might influence the floor acceleration response at several locations compared to the response of the actual structure. However, the purpose of this article is to test how different sets of records selected according to different IMs affect the response of SSCs mounted in the reactor building. This goal is not obstructed by an approximate estimation of the floor accelerations.

2.2 Soil-structure interaction

The structural response of the reactor building was computed accounting for soil-structure interaction. In this framework, the ground is represented by impedance functions which can be seen as a boundary condition applied to the interface with the ground of the structural model.

We characterized the soil using the best-estimate stratified profile (Figure 4) based on geotechnical data derived from the METIS case study c'site of interest.

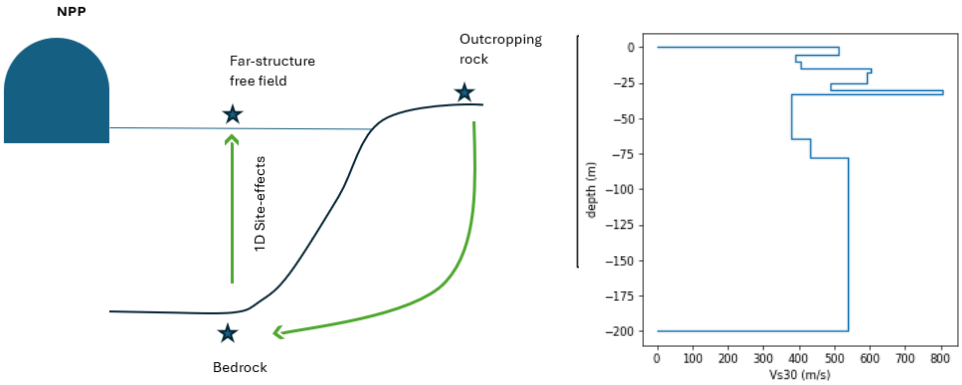

Figure 4: Methodology to introduce site response and account for SSI (left) and best-estimate soil profile (right)

Note that as input to the soil amplification analysis we use rock ground motions extracted from the available databases without any deconvolution to bedrock conditions. In other words, for simplicity we consider that the outcrop rock ground motions and bedrock ground motions are identical, which is an assumption that holds for very rigid rock conditions. This approximation is tenable given the limited objective of this study. The ground is modeled through impedance functions which can be seen as a boundary condition applied to the interface with the ground of the structural model.

3. CASE STUDY SITE, HAZARD ANALYSIS AND GROUND MOTION RECORD SELECTION

We assume the nuclear installation to be located at a site in Tuscany, Italy. We use results from METIS case study PSHA (Chartier & Rood, 2024) developed with the OpenQuake engine (Pagani et al. 2014) . For this particular study, we select IM=PGA and IM*=Sa (0.25s) of the horizontal components of the ground motion as the IM* to predict the floor acceleration responses of the reactor building. Figure* 5 *displays the hazard curves of the intensity measures used for this study and related uniform hazard spectra. To perform multiple stripe analysis (MSA), we use the sets of CS developed in METIS project based on the CS approach (Sipcic et al. 2023). This method accounts for hazard consistency in the horizontal spectral ordinates, as discussed in previous studies (Jayaram et al. 2011; Lin, Haselton and Baker 2013). For simplicity, the vertical component was not included in the selection procedure but the procedure might be extended to vertical spectral ordinates, as discussed by Kohrangi et al. (2023). We perform record selection for ten different IM levels (IMLs) corresponding to different return periods.*

Table 2 summarizes the different IML values for each conditioning IM*.

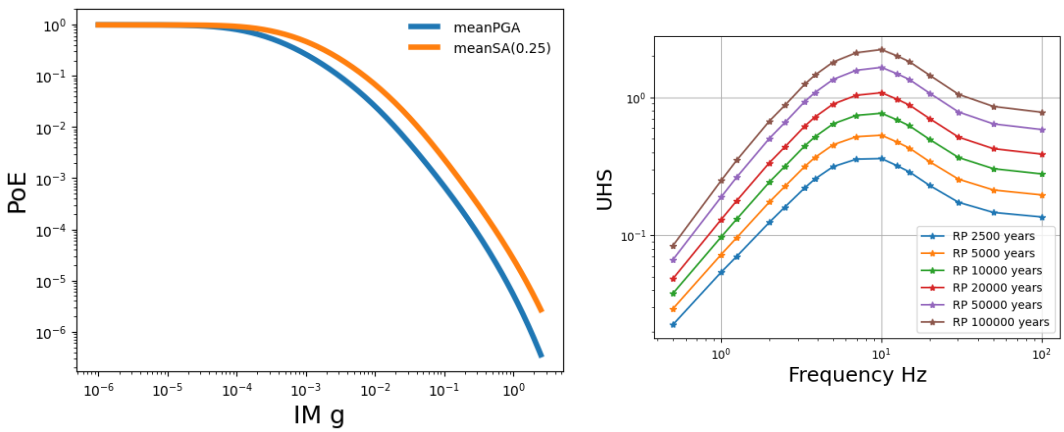

Figure 5: Hazard curves for the two selected IM$_1$=PGA and IM*$_2$=Sa (0.25s) (left) and UHS for six return periods*

Table 2: IML values for different return periods

IML	1	2	3	4	5	6	7	8	9	10
Return period	40	150	475	1000	2500	5000	10000	20000	50000	100000
IM*=PGA (g)	0.01	0.025	0.051	0.079	0.132	0.191	0.27	0.377	0.565	0.752
IM*=Sa (0.25s) (g)	0.021	0.052	0.104	0.157	0.257	0.368	0.519	0.721	1.08	1.44

4. STRUCTURAL RESPONSE ASSESSMENT

This section presents some of the selected results obtained from TF (transfer function analysis) and MSA (Multiple stripe analysis). For each run, we monitor EDPs, including the maximum peak floor acceleration and the floor spectral acceleration for a wide range of frequencies in all three directions and at four selected levels (1st level: 6 meters, 2nd level: 12meters, 3rd level:37 meters and 4th level at 64 meters-dome) in the base part of the reactor locations (see Figure 6).

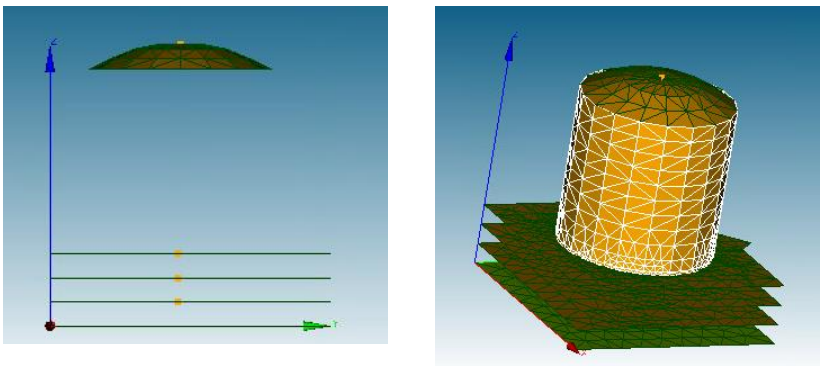

Figure 6: post-processing points of the structural model

4.1 TRANSFER FUNCTION

In this first subsection, we discuss the results of the TF analysis. We perform TF analysis to understand better the dynamic behavior of the reactor building and the locations at which we expect high floor acceleration demands. The TF analysis is performed in code-aster by inputting a uniform unitary frequency signal and measuring the response and amplification at different spectral frequencies at various locations. Figure 7 shows the TF at different frequencies for different reactor locations (4 different levels at elevation) and in three different directions. We observe that the amplification is more evident at the top floors. The amplification in the vertical direction is also of high importance.

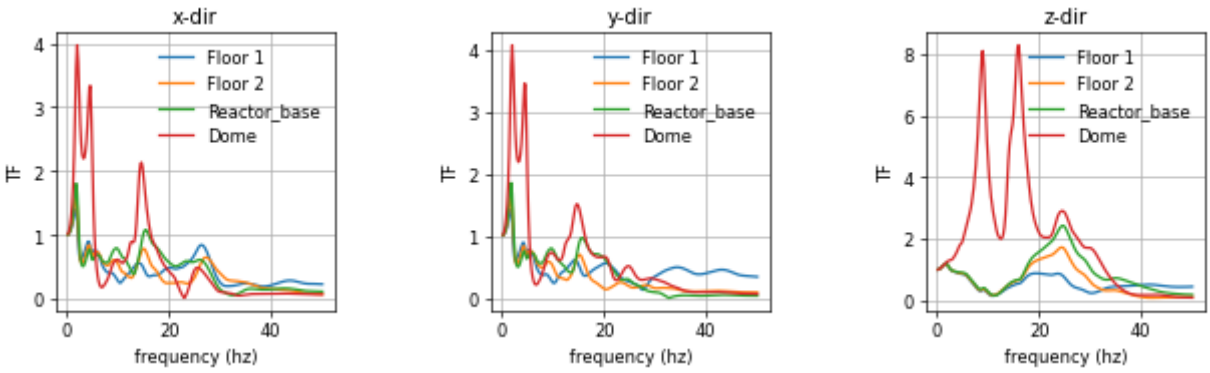

Figure 7: TF along height for different directions; x-direction (left), y-direction (middle) and z-direction (right)

4.2 MULTIPLE STRIPE ANALYSIS AND SENSITIVITY OF THE FLOOR ACCELERATION RESPONSE ON THE CONDITIONING IM

For this study, we run the two sets of ground motions associated with the five stripes from 5 to 9 listed in Table 2 that were selected based on the CS approach with IM*$_1$=PGA and IM*$_2$=Sa(0.25s) as conditioning IMs. As an illustrative example, Figure 8 shows the ground motion time histories, the floor response acceleration time history and the floor response spectra for three different directions at the base of the building for a particular ground motion record. We observe higher spectral amplifications at frequencies between 5-10Hz, especially in the x-direction.

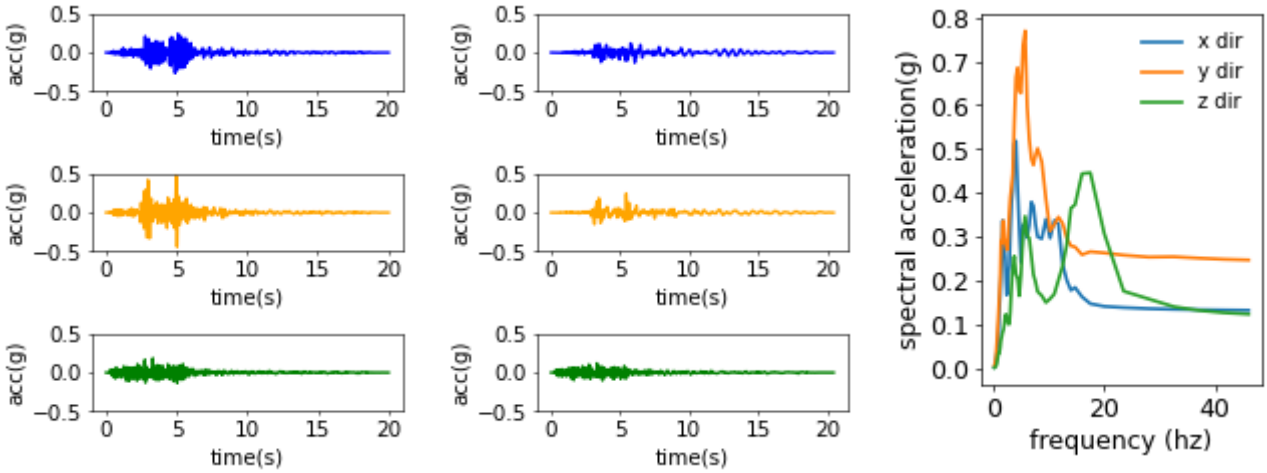

Figure 8: Single ground motion record plots (IML_8/Coalinga, RSN401, sequence number 401); ground motion time histories (first column); floor acceleration time histories (second column); floor acceleration response spectra (third column). The time histories in the first, second and third rows refer to x, y, and z directions, respectively.

Figure 9 (left) shows the median floor spectral acceleration (FSA) at 100Hz (similar to PFA) at the dome of the building using the two sets of ground motion records. The estimates of the median FSA seem to have minor sensitivity to the choice of the conditioning IM*. However, the dispersion of the response at the dome in each one of the three directions (Figure 9, middle) is very sensitive to the selected IM*. As a matter of fact, the sensitivity of the IM* on the dispersion varies from location to location. IM*$_2$ seems to better predict the floor response at the highest levels, while both IM*s seem good indicators for the floor responses closer to the ground (Figure 9, right).

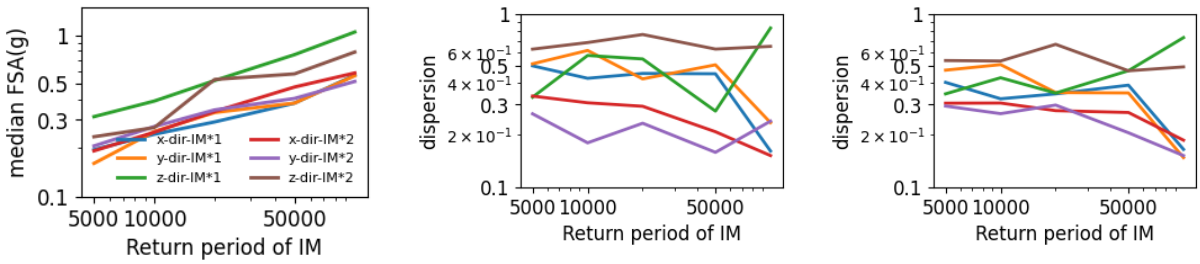

Figure 9: MSA-Sensitivity of the floor spectral acceleration (FSA) response to the conditioning IM; from left to right, median (left) and dispersion (middle) @ 4th level-dome; dispersion @ 1st level (right)

5. Sensitivity of SSC fragility curves to conditioning IM and to response analysis set-up

Seismic fragility curves for a given limit state (e.g., failure) provide the conditional probability that the engineering demand parameter (EDP, here called generically y) exceeds a threshold, y_{crit} , associated with the onset of the limit state for a given level of ground motion intensity, a:

$$P_f(a) = P(y > y_{crit}|a) \tag{3}$$

When the widely adopted lognormal fragility model proposed in (Kennedy et Al. 1980; Huang et Al. 2011, Zentner et al 2016) is applied, the shape of the fragility curve is approximated by the cumulative distribution function of a lognormal distribution:

$$P_f(a) = \Phi\left(\frac{lna - ln\widehat{A_m}}{\beta_R}\right) \tag{4}$$

where Φ is the CDF of the standard normal distribution and $\widehat{A_m}$ denotes the median capacity. The parameter β_R, which represents the uncertainty, is the standard deviation of the median capacity.

In this study, we derive fragility curves for the failure of an equipment located on ….. The damage measure is the average of the maximum floor spectral accelerations of the two horizontal directions, between 5 to 9 Hz, i.e., AvgSa (5:1:9) that we adopted as the EDP to gauge the equipment performance. For the purpose of this study, we assume two reduced failure thresholds, y_{crit}={0.4g,0.7g}, lower than typical failure thresholds for nuclear equipment, to better illustrate some aspects of the fragility modeling procedure.

In the next two sections we will investigate the sensitivity of both $\widehat{A_m}$ and β_R to a) the IM* of the rock ground motions and b) to the analysis set-up, namely MSA and cloud (a.k.a. regression) analysis.

5.1 FRAGILITY ANALYSIS METHODS

There are different ways to derive fragility curves but here we consider only multiple stripe analysis (MSA) and cloud analysis (Zentner, Gündel and Bonfils, 2016). We derive fragility curves based on MSA outputs presented in the previous section, and we also use the IM-EDP pairs of MSA to perform cloud analysis.

We first explain the procedure with MSA. We estimate the probability that the EDP exceeds the capacity threshold at each stripe. We can calculate Probabilities of Exceedance (PoEs) by counting the exceedances of the specific EDP at each stripe or by fitting a lognormal model at each stripe. The final step is to fit a lognormal model to the PoEs' Empirical Cumulative Density Function (ECDF).

The alternative way is to use the IM-EDP pairs coming from MSA and perform cloud analysis. Under the assumption that the IM-EDP relationship is lognormal, we fit a linear regression model in the lognormal space to establish a relationship between IM-EDP. We estimate the standard error of estimation and use it as the conditional dispersion along the regression line. We then evaluate the PoEs for different points across the regression line and fit a lognormal curve (Zentner, Gündel and Bonfils, 2016).

For the MSA, the IM used for evaluating the fragility curves must be the same as the conditioning IM* utilized in record selection. This is not the case for the regression approach. Any record selection procedure can be used. In particular, both IM* sets can be used together for the regression (provided that the two sets do not have ground motions in common, as is the case here). Consequently, the regression approach can be easily extended to the vector fragility case, which is one of the reasons why it is considered here in addition to MSA.

5.2 SENSITIVITY ANALYSIS ON THE CONDITIONING IM*

First, we explore the sensitivity analysis of the conditioning IM* on SSC's fragility curves (computed via MSA). Figure *10* displays the fragility curves of the equipment for two different conditioning IM*. We also explore the differences in fitting a lognormal model to the ecdf of PoEs estimated by counting the exceedances (direct) or by fitting a lognormal model to the EDPs at each return period. In the two panels in the first row, we see the fragility curves of an SSC located at the 1st level (1st floor). As mentioned earlier, we assume a failure threshold of 0.4g. The 1st panel corresponds to the case in which we fit the lognormal model to the PoEs, which are calculated by counting the exceedances. The 2nd panel refers to the case in

which we fit at each stripe a lognormal distribution to the PoEs. The differences between the fragility parameters of the first row's panels are minor. On the second row, we see the fragility curves of the same SSC with a failure threshold of 0.7g. We observe that since the number of failures is very low, we get smaller PoEs, and thus the fit of a lognormal curve is not very robust. This is evident from the large differences in the fragility parameters between the two panels (PoEs from fitting a lognormal model-left and from direct estimation-right) of the second row. We observe some differences in the fragility curves' slope when considering different conditioning IM*s.

The final check that we perform is to take the hazard-consistent ground motion sets of IML7 (10000 years return period) for the two conditioning IM*s and perform Incremental Dynamic Analysis (IDA) (Vamvatsikos and Cornell, 2002) at the acceleration levels corresponding to IML5-9.

The third row of Figure *10* represents the fragility curve of an SSC located at the 1st floor with a failure threshold of 0.4g (same as the first row of the same figure) after the scaling of the ground motion set. The fragility parameters are similar to the case in which we consider a fully hazard-consistent spectral shape at all IML's. A summary of all parameters is illustrated in Table 3.

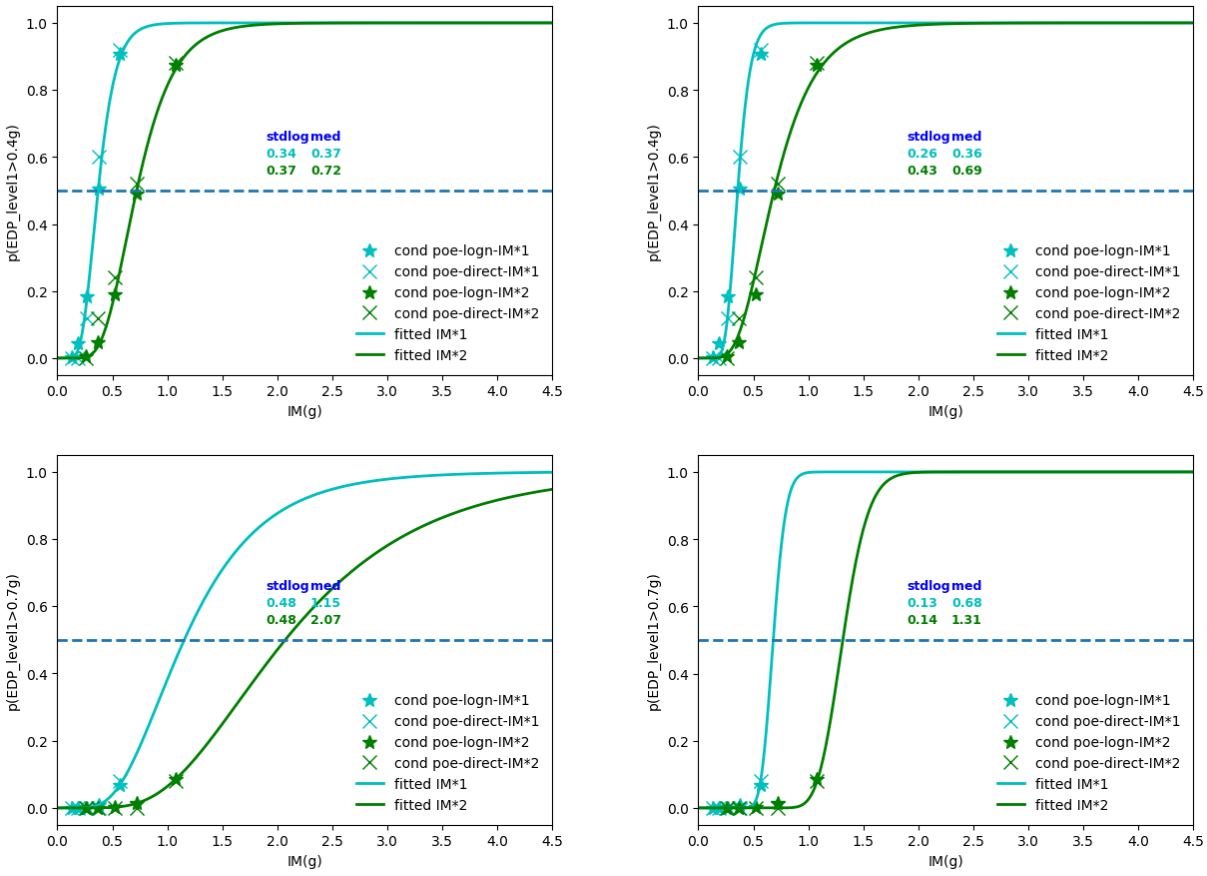

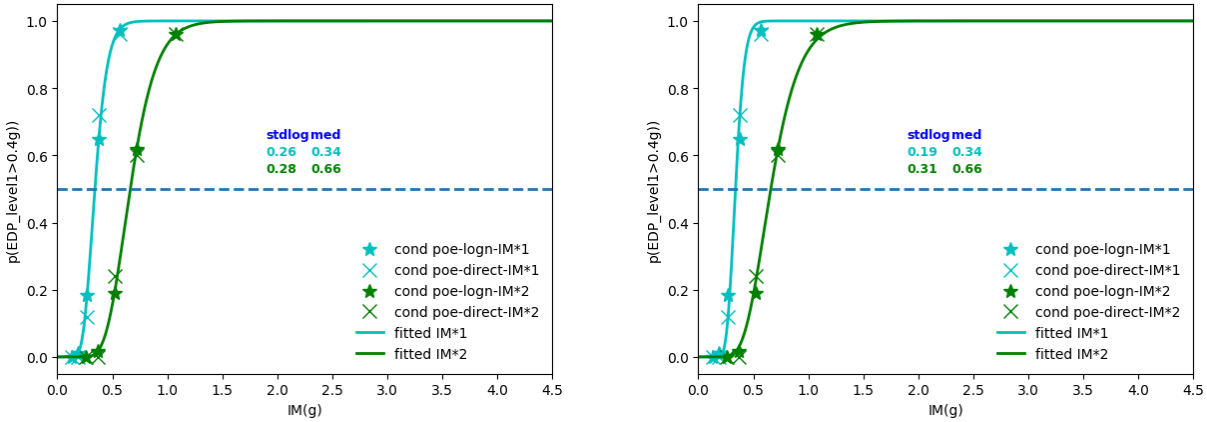

Figure 10*: Fragility curves comparison for the two different conditioning IM*s ; first row: fragility curves of component @ level1 with an assumed failure threshold of 0.4g; second row: fragility curves of component @ level1 with assumed failure threshold of 0.7g; third row: fragility curves of component @ level1 with assumed failure threshold of 0.4g based on scaled MSA-IML7 set; first column: estimation of PoEs with a lognormal model; second column: estimation of PoEs with direct estimation of exceedances*

*Table 3: Comparison of fragility parameters for the two conditioning IM*s (PGA and SA(0.25)*

Intensity measure (IM*)	Fragility parameters							
	Lognormal PoEs				Direct PoEs			
	$\widehat{A_m}$		β_R		$\widehat{A_m}$		β_R	
	IM^*_1	IM^*_2	IM^*_1	IM^*_2	IM^*_1	IM^*_2	IM^*_1	IM^*_2
MSA-threshold 0.4g	0.37	0.72	0.34	0.37	0.36	0.69	0.26	0.43
MSA-threshold 0.7g	1.15	2.07	0.48	0.48	0.68	1.31	0.13	0.14
Scaled MSA-threshold 0.4g	0.34	0.66	0.26	0.28	0.34	0.66	0.19	0.31

5.3 SENSITIVITY ANALYSIS ON THE ANALYSIS METHOD, MSA VS CLOUD ANALYSIS

The scope of this subsection is to perform a sensitivity analysis of the fragility curves to the method analysis set-up (MSA vs cloud analysis) adopted for estimating the response. As we describe in the previous section, to perform regression analysis, we need to use the IM-EDP pairs from MSA. We already have two datasets from the CS-MSA for the two different conditioning IM*s. To perform the regression analysis, we can use either the dataset from each conditioning IM* separately or merge the two different datasets. Figure 11 displays the fitted regression lines based on the three cases, the first two for each distinct dataset of MSA, and the third one corresponds to the merged dataset. We observe that the regression outputs are somewhat insensitive to the dataset selection indicating the robustness of the approach.

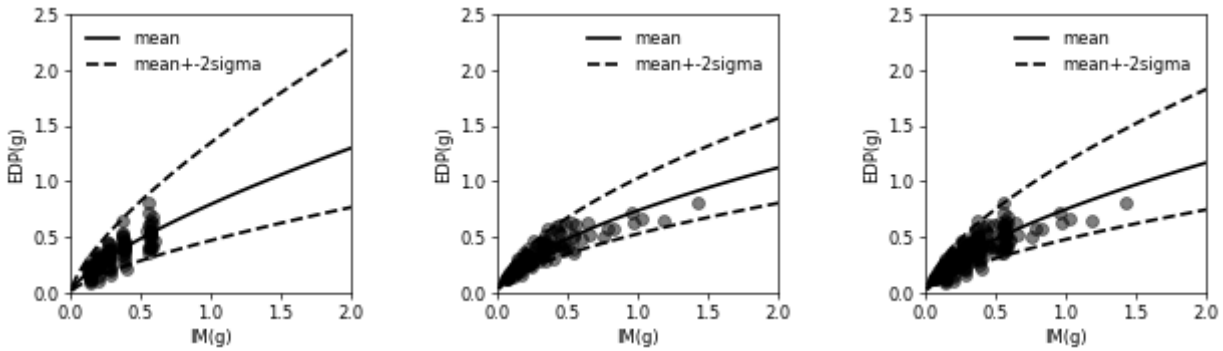

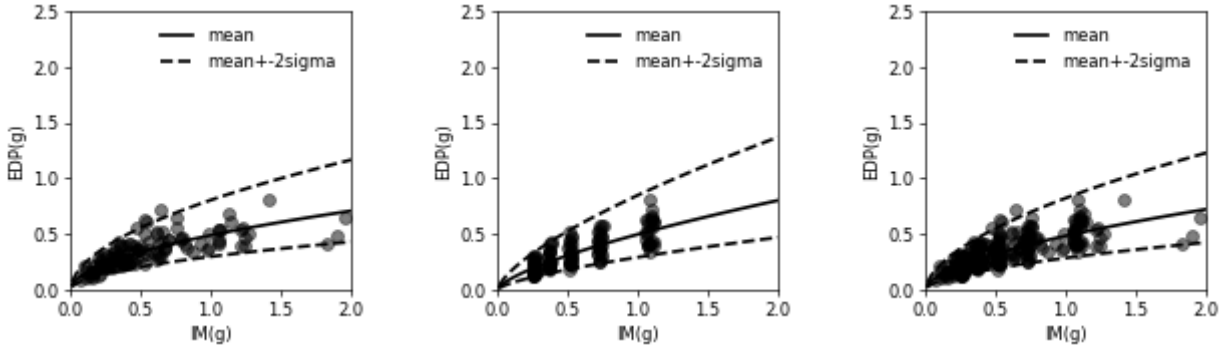

Figure 11: regression plots (IM-EDP)-sensitivity to the dataset selection; first row corresponds to IM=Sa(0.01s) for the two different datasets and the merged one; second row corresponds to IM=Sa(0.25s); from left to right, MSA-IM*=Sa(0.01s), MSA-IM*=Sa(0.25s) and merged dataset.; SSC located @ 1st level with an assumed failure threshold of 0.4g;

The next step is to derive fragility curves based on regression analysis carried out on the cloud of data. This presupposes that we can estimate the PoEs. For that, we adopt the classical lognormal relation between the EDP and the IM (Zentner et al. 2016). Note that the standard error is constant along the regression line and doesn't change with the level of intensity in the log-space (it does increase in the physical space as can be seen in Figure 11 mainly due to increased ground motion variability at higher return periods).

The last part of this subsection compares the fragility curves based on regression analysis and MSA. We are comparing the case of IM^*_1=Sa(0.01s) and IM^*_2=Sa (0.25s), each for the three different datasets used. The first row of this figure corresponds to IM^*_1 and the second row to IM^*_2. We observe very little differences between MSA and regression fragility curves (Figure 12). As a final check, we also use risk metrics to compare the efficiency of the different methods by integrating the fragility and the hazard curves. Table 4 compares the annual rate of exceeding this damage state (for SSC located @ 1st level with an assumed failure threshold of 0.4g) for the different approaches (for the regression method, we show just the case with the merged dataset). The discrepancy in the risk estimates, which theoretically should be identical but differ due to the limited ground motion sample size utilized here, are minor and negligible for all practical purposes.

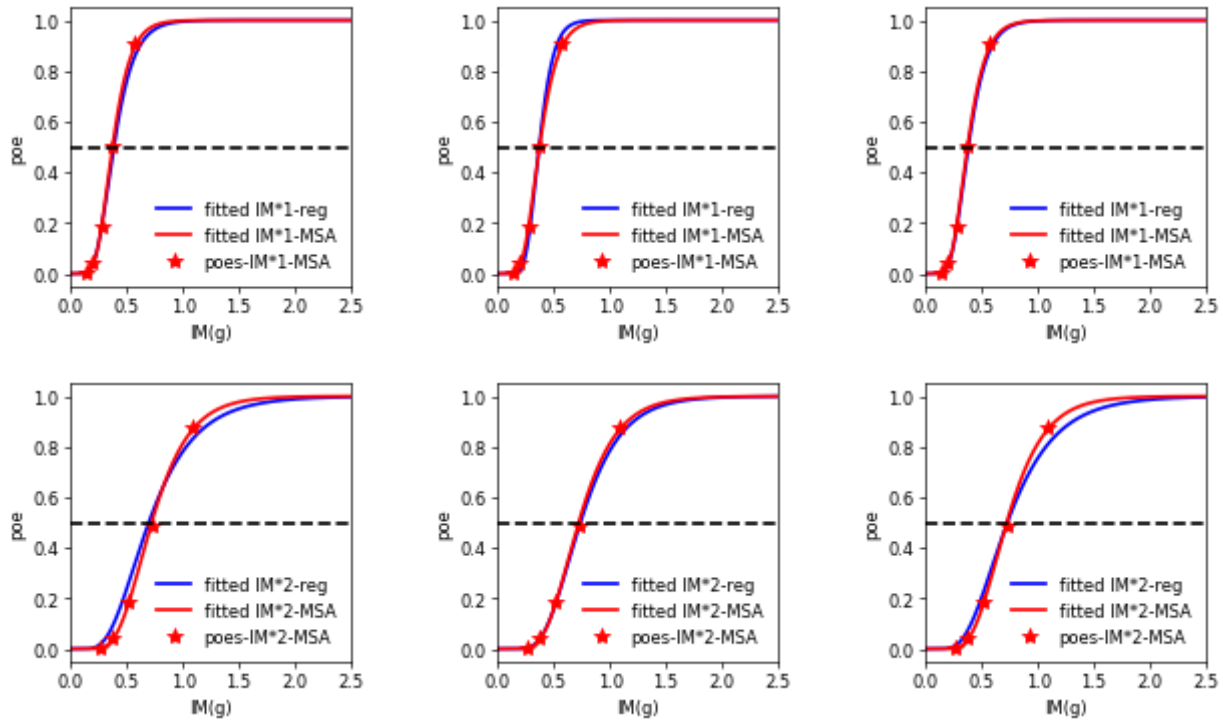

Figure 12: Comparison of fragility curves for MSA and regression analysis; comparison for IM^*_1=Sa(0.01s (top) and IM^*_2=Sa (0.25s) (bottom) for the three different datasets; from left to right, IM*=Sa(0.01s), IM*=Sa(0.25s) and the merged dataset; SSC located @ 1st level with an assumed failure threshold of 0.4g;

Table 4: Annual rates of exceeding the damage state (failure); SSC located @1st level with an assumed failure threshold of 0.4g;

Intensity measure (IM*)	λ × 10e+05	Fragility parameters	
		$\widehat{A_m}$	β_R
Sa(0.01s)-MSA	6.99	0.37	0.34
Sa(0.25s)-MSA	6.98	0.72	0.37
Sa(0.01s)-reg/merged	6.77	0.38	0.35
Sa(0.25s)-reg/merged	7.99	0.73	0.46

6. VECTOR IMS-DISCUSSION

One of the objectives of this study is to lay the foundations for introducing a new approach that includes vector IMs in the seismic risk analysis of nuclear power plants. As stated earlier, we reiterate here that in the framework of probabilistic seismic risk analysis (PRA) of nuclear power plants, a single ground motion intensity measure (IM) is generally used as a predictor of the performance of structures, systems, and components (SSCs) subject to earthquakes. In most cases, Peak Ground Acceleration (PGA) is the IM of choice.

Several studies (Soroushian et al. 2016; Ryan et Al 2016) have shown that there are components that are sensitive to vertical floor accelerations. In nuclear engineering practice, several SSCs are sensitive to the vertical floor acceleration demand. To better predict vertical floor acceleration demands and reduce the variability in the fragility curves of those SSCs, a vector IM that includes both the horizontal and the vertical component of the ground motion can be used. This will be the object of further analysis conducted by the authors.

7. CONCLUSIONS

We explored the sensitivity of the conditioning IM* when we used the CS approach on the floor acceleration response of a nuclear power plant and in the estimation of the fragility curves of SSC. Our findings suggest that the slope of the fragility curve is sensitive to the conditioning IM. The choice of the IM had a minor impact on the total failure rates.

The results in terms of risk show negligible differences that could probably be reduced even further if one is willing to increase the sample size of the ground motions utilized for response assessment. Moreover, we used the data from MSA analysis to perform a regression analysis between several IM*s and the EDP of interest. We used the regression outputs to estimate PoEs and fitted lognormal fragility curves. The fragility curves obtained from MSA and cloud analysis are very similar. The robustness of these results will be tested using more SSCs and different analysis set-ups.

8. ACKNOWLEDGEMENTS

The authors gratefully acknowledge the financial support by the European Commission through the Program METIS with grant agreement number: 945121 (HORIZON 2020) to this work. The authors would like to thank our colleague from EDF, Dzifa Kudawoo for his contribution in the structural modeling of the ZNPP model in code-aster.

9. REFERENCES

Bradley B.A. (2010) ‘A generalized conditional intensity measure approach and holistic ground-motion selection’, *Earthquake Engineering & Structural Dynamics*, 39(12), pp. 1321–1342. Available at:

https://doi.org/https://doi.org/10.1002/eqe.995.

'code_aster - opensource Finite element software'. Available at: https://code-aster.org/V2/spip.php?rubrique2.

Salome-Meca : une plate-forme au service de la simulation mécanique. Available at: https://code-aster.org/V2/spip.php?article303.

EPRI (1991) *EPRI, 1991. Generic Seismic Ruggedness of Power Plant Equipment (Revision 1). Technical Report; Electric Power Research Institute EPRI, Palo Alto, CA.*

Huang Y.-N., Whittaker A.S.,Luco N. (2011) 'A probabilistic seismic risk assessment procedure for nuclear power plants: (I) Methodology', *Nuclear Engineering and Design*, 241(9), pp. 3996–4003. Available at: https://doi.org/https://doi.org/10.1016/j.nucengdes.2011.06.051.

Jayaram N., Lin T. and Baker J.W. (2011) 'A Computationally Efficient Ground-Motion Selection Algorithm for Matching a Target Response Spectrum Mean and Variance', *Earthquake Spectra*, 27(3), pp. 797–815. Available at: https://doi.org/10.1193/1.3608002.

Kennedy R.P.,Cornell C.A., Campbell R.D., Keplan S.,*Perla H.F.* (1980) 'Probabilistic seismic safety study of an existing nuclear power plant', *Nuclear Engineering and Design*, 59(2), pp. 315–338. Available at: https://doi.org/https://doi.org/10.1016/0029-5493(80)90203-4.

Kohrangi, M.*, Bakalis K., Triantafyllou G., Vamvatsikos D.,Bazzurro P.* (2023) 'Hazard consistent record selection procedures accounting for horizontal and vertical components of the ground motion: Application to liquid storage tanks', *Earthquake Engineering & Structural Dynamics*, 52(4), pp. 1232–1251. Available at: https://doi.org/10.1002/EQE.3813.

Lin, T., Haselton, C.B. and Baker, J.W. (2013) 'Conditional spectrum-based ground motion selection. Part I: Hazard consistency for risk-based assessments', *Earthquake Engineering & Structural Dynamics*, 42(12), pp. 1847–1865. Available at: https://doi.org/https://doi.org/10.1002/eqe.2301.

Chartier, T., & Rood, A. (2024). METIS D4.6 - Preparation of the METIS study case (WP4) and application. Zenodo. https://doi.org/10.5281/zenodo.10529417(available at https://metis-h2020.eu/deliverables)

Pagani M, Monelli D, Weatherill G, Danciu L, Crowley H, Silva V, *et al.* (2014) 'OpenQuake Engine: An Open Hazard (and Risk) Software for the Global Earthquake Model', *Seismological Research Letters*, 85, pp. 692–702. Available at: https://doi.org/10.1785/0220130087.

Ryan KL, Soroushian S, Maragakis E "Manos," Sato E, Sasaki T, Okazaki T. (2016) 'Seismic Simulation of an Integrated Ceiling-Partition Wall-Piping System at E-Defense. I: Three-Dimensional Structural Response and Base Isolation', *Journal of Structural Engineering*, 142(2), p. 04015130. Available at: https://doi.org/10.1061/(asce)st.1943-541x.0001384.

Šipčić Nevena, García de Quevedo Iñarritu Pablo, Kohrangi Mohsen, Bazzurro Paolo (2023) *Methodology for selecting ensembles of hazard-consistent ground motions suitable for fragility curve computations for clustered seismicity and datasets for WP6-D5.2*. Available at: https://metis-h2020.eu/wp-content/uploads/2023/06/D5_2_Methodology_for_selecting_ensembles_of_rock_hazard_consistent_ground_motions_suitable_br___for_fragility_curves_computations_for_clustered_seismicity_and_dataset_V2.pdf.

Soroushian S, Maragakis E "Manos", Ryan KL, Sato E, Sasaki T, Okazaki T, *et al.*(2016) 'Seismic Simulation of an Integrated Ceiling-Partition Wall-Piping System at E-Defense. II: Evaluation of Nonstructural Damage and Fragilities', *Journal of Structural Engineering*, 142(2), p. 04015131. Available at: https://doi.org/10.1061/(asce)st.1943-541x.0001385.

Spillatura A., *Kohrangi M., Bazzurro P., Vamvatsikos D.* (2021) 'Conditional spectrum record selection faithful to causative earthquake parameter distributions', *Earthquake Engineering & Structural Dynamics*, 50(10), pp. 2653–2671. Available at: https://doi.org/https://doi.org/10.1002/eqe.3465.

Vamvatsikos, D. and Cornell, C. (2002) 'Incremental Dynamic Analysis', *Earthquake Engineering & Structural Dynamics*, 31, pp. 491–514. Available at: https://doi.org/10.1002/eqe.141.

Zentner I., Gündel M., and Bonfils N. (2016) 'Fragility analysis methods: Review of existing approaches and application', *Nuclear Engineering and Design*, 323. Available at: https://doi.org/10.1016/j.nucengdes.2016.12.021.

Trevlopoulos, Konstantinos & Zentner, Irmela. (2020). Seismic Fragility Curve Assessment Based on Synthetic Ground Motions with Conditional Spectra. Pure and AppliedGeophysics. 177.